Preferential CO oxidation over nanosized gold catalysts supported on ceria and amorphous ceria–alumina

Juliana Fonseca[a,b], Sébastien Royer[a], Nicolas Bion[a], Laurence Pirault-Roy[a], Maria do Carmo Rangel[b], Daniel Duprez[a], Florence Epron[a,*]

[a] Institut de Chimie des Milieux et Matériaux de Poitiers, Université de Poitiers, UMR 7285 CNRS, B27, 4 rue Michel Brunet, 86022 Poitiers cedex, France
[b] GECCAT Grupo de Estudos em Cinética e Catálise, Instit. de Química, Universidade Federal da Bahia, Campus Universitário de Ondina, Salvador, BA, Brazil

ARTICLE INFO

ABSTRACT

1 wt.% Au supported on CeO_2–Al_2O_3 (Ce/Ce + Al: 0, 2, 5, 10, 15, and 20 mol%) was prepared by impregnation in organic medium of high-surface area supports prepared by Evaporation Induced Self Assembly (EISA) route. For comparison, a 1 wt.% Au/CeO_2 was also prepared using a commercial support. All the prepared catalysts present a BET surface area roughly between 200 and 340 m^2 g^{-1}. The reducibility, the oxygen storage capacity (OSC) and the oxygen mobility determined by oxygen isotopic exchange (OIE) of the 1 wt.% Au/CeO_2–Al_2O_3 are enhanced by the presence of gold and increases with the cerium content in the support. The values of the OSC and the oxygen mobility in the Au/CeO_2–Al_2O_3 catalysts with high cerium loading are higher than those determined on their Au/CeO_2 counterpart. The activity in CO oxidation of the Au/CeO_2–Al_2O_3 catalysts increases with the cerium content in the support, which could be linked to the better oxygen mobility of these systems, whereas in CO-PrOx the Au/CeO_2–Al_2O_3 catalysts with medium cerium loading (Ce/Ce + Al = 5 and 10 mol%) present the highest CO conversion at 50–60 °C. The catalysts are stable at 100 °C in $CO + O_2 + H_2$ mixtures. The addition of CO_2 in the stream strongly deactivates Au/CeO_2, whereas Au/CeO_2–Al_2O_3 is less affected. Whatever the catalyst, the presence of steam has no significant effect on the catalytic performances.

© 2012 Elsevier B.V. All rights reserved.

1. Introduction

Proton-exchange membrane (PEM) fuel cell technology is very promising for replacing internal combustion engines for transportation applications, but needs the use of hydrogen containing less than 100 ppm of CO to avoid the poisoning of the electrodes. In these devices, carbon monoxide acts as a poison, due to its strong adsorption on the platinum or platinum–ruthenium anodic electrocatalysts, which inhibits the adsorption of hydrogen in these cells and lowers their performances [1,2].

The main processes used for H_2 production are the natural gas and naphtha steam reforming, followed by a two-step water gas shift (WGS) reaction, which increases the hydrogen yield while decreasing the CO content. Final purification can be achieved by various processes, such as the preferential CO oxidation (CO-PrOx), performed in the 25–200 °C temperature range. This reaction was first suggested in 1921 as an economic process for the removal of carbon monoxide from hydrogen containing streams [3,4] and it is nowadays applied to the purification of hydrogen in fuel cells type such as PEM fuel cells.

In the CO-PrOx process, CO oxidation (Eq. (1)) is the desired reaction while H_2 oxidation (Eq. (2)) should be avoided.

$$CO + (1/2)O_2 \rightarrow CO_2 \tag{1}$$

$$H_2 + (1/2)O_2 \rightarrow H_2O \tag{2}$$

At temperatures higher than 150 °C, the oxidation reactions may be accompanied by reverse water-gas shift (Eq. (3)) and/or CO methanation (Eq. (4)) reactions:

$$CO_2 + H_2 \rightarrow CO + H_2O \tag{3}$$

$$CO + 3H_2 \rightarrow CH_4 + H_2O \tag{4}$$
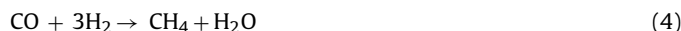
Since the discovery of the exceptional catalytic properties of nanosized supported gold particles, with diameters of 2–3 nm, in the low-temperature CO oxidation reaction [5–7], Au catalysts have been the subject of numerous investigations for total and preferential CO oxidation [8,9]. The advantage of gold catalysts over other noble metal catalysts such as platinum, ruthenium or rhodium, is that supported gold catalysts are much more active for CO oxidation than for H_2 oxidation, which is the researched property for the CO-PrOx reaction [10]. On gold, the active sites for CO adsorption are

* Corresponding author. Tel.: +33 5 49 45 48 32; fax: +33 5 49 45 37 41.
E-mail address: florence.epron@univ-poitiers.fr (F. Epron).

the low coordination surface atoms [11,12], and more precisely Au sites with coordination number ≤ 7 [13]. For the CO-PrOx reaction, the support plays also a crucial role and gold nanoparticles are very often supported on active or reducible materials like TiO_2 [14,15], Fe_2O_3 [16,17], MnOx [18,19], and CeO_2 [20,21], which are able to provide oxygen atoms during the catalytic reaction. Thus, gold catalysts supported on cerium oxide have been widely studied in the CO-PrOx reaction due to the ability of ceria to store and/or provide oxygen atoms [17,22–28]. On Au/CeO_2 catalysts, it was proposed that the CO oxidation reaction occurs between CO adsorbed on gold nanoparticles and oxygen atoms coming from the dissociation of oxygen molecules on reduced ceria at the ceria–gold interface [29]. It has been shown that gold supported on nanocrystallites of CeO_2 is much more active than that supported on large CeO_2 crystallites [30]. However, CeO_2 support presents a poor thermal stability against sintering. For this reason, CeO_2–Al_2O_3 type oxides are widely studied as catalyst supports in various oxidation reactions, for which alumina plays an essential role in structural and thermal stability of the catalysts. The presence of alumina increases the oxygen storage capacity as well as the stability of supported noble metal particles and ceria itself, avoiding the phenomenon of agglomeration [31].

However, the addition of ceria to alumina by the simple impregnation method limits the amount of ceria deposited. Therefore, to increase the interaction of ceria with alumina in CeO_2–Al_2O_3 oxides, various preparation methods have been extensively studied. Among them, the sol–gel method has proven to be a promising approach. In a study using this method [32], catalysts containing different amounts of cerium oxide (from 2 to 50 wt.% CeO_2 in aluminum oxide) were prepared, impregnated with noble metals (palladium and platinum) and evaluated in methane oxidation. In the case of samples containing between 2 and 15 wt.% CeO_2, it was observed that the higher the cerium content, the lower the catalytic activity. This phenomenon was attributed to the oxidation of noble metal caused by the presence of ceria. On the other hand, the catalyst containing platinum and 50 wt.% CeO_2 was the most active, which was related to the higher mobility of oxygen in this sample. According to the authors, the support preparation by sol–gel method presents several advantages, as compared to impregnation methods: (i) larger amounts of ceria, keeping relatively high specific surface areas, (ii) stronger interaction between the support and the metal and (iii) high homogeneity and thermal stability.

The co-precipitation method has also been used for synthesizing these materials. For example, Aresta et al. [33] have obtained mixed oxides containing different quantities of aluminum and cerium. The catalysts were evaluated in the direct carboxylation of methanol. It was observed a reduction of the loss of ceria specific surface area during the reaction and an inhibition of the deactivation of catalyst with the aluminum addition to the ceria.

Since the intensive development of mesostructuration routes during the last 20 years, various oxides and mixed oxides exhibiting improved physical properties and organized porosity have been obtained using ionic or non ionic/neutral templating agents. Recently, CeO_2–Al_2O_3 mesoporous mixed-oxides were synthesized by Evaporation Induced Self Assembly (EISA) route [34]. Ceria nanoparticles (3–5 nm) supported on alumina with highly organized structures and high specific surface areas were obtained. They were used as supports for gold catalysts in the oxidation of carbon monoxide and gave higher catalytic activity than Au/CeO_2 catalyst, showing CO conversion of 100%, at room temperature. The aim of the present study is to evaluate the redox properties, oxygen mobility and the activity in CO oxidation, in the presence or not of hydrogen of gold catalysts supported on Ce–Al oxides prepared by sol–gel method. This method is expected to produce highly dispersed ceria particles and very active catalysts in the CO-PrOx reaction.

2. Experimental

2.1. Catalysts preparation

The pure alumina support was synthesized similarly to the method described by Yuan et al. [35]. The triblock copolymer Pluronic P123 ($EO_{20}PO_{70}EO_{20}$), structuring agent, was dissolved in ethanol (99.9%). Nitric acid (90%), and aluminum isopropoxide (98%) were then added to the first solution. After stirring and evaporation in an oven at 60 °C (5 days), the sample was ground and calcined at 600 °C, for 4 h (1 °C min^{-1}, 40 mL min^{-1} O_2). The derived mesoporous ceria–alumina supports were synthesized by the same method, by substitution of a part the aluminum isopropoxide by cerium acetate (>98%) in order to obtain samples with 2, 5, 10, 15 and 20 mol% of cerium (Ce/Ce + Al ratio). These samples were calcined at 400 °C. In the following, this support series will be noticed CeXAl, with X = Ce/Ce + Al molar percentage. Ceria with high specific surface area also used in this work was supplied by Rhodia.

Gold catalysts were prepared by impregnation in organic medium under argon atmosphere, as described in Ref. [28]. The gold precursor was dimethyl(acetylacetonate)gold(III) [Au(acac)$_3$] supplied by Strem Chemical. Before the impregnation, 0.5 g of the support was pre-treated under flowing Ar (60 mL min^{-1}), at 400 °C for 2 h, at a heating rate of 2 °C min^{-1} and cooled down to room temperature. It was first immersed in 10 mL toluene, then 10 mL of Au(acac)$_3$ in solution in toluene was added, and kept for 6 h at 40 °C under bubbling Ar. The amount of Au(acac)$_3$ dissolved in toluene corresponded to 1 wt.% of gold. Toluene was drained from the sample that was dried under argon flow during 15 h, at 40 °C. The samples were calcined for 1 h at 300 °C (2 °C min^{-1}), under flowing air (30 mL min^{-1}). The chemical composition was obtained by ICP-OES using a Perkin Elmer Optima 2000 DV. The samples were mineralized with a mixture of nitric and chloride acid and the results of this analysis are shown in Table 1.

2.2. Specific surface area measurements

The specific surface area measurements were carried out by nitrogen adsorption at −196 °C, in a Micromeritics equipment, model TRISTAR 3000. The specific surface areas were calculated using the BET (Brunauer–Emmett–Teller) model. For the analysis, about 0.1 g of the sample was heated up to 250 °C, for 2 h, under vacuum in order to remove the adsorbed species. For the analysis of gold samples, the reactor was covered with aluminum foil to prevent the incidence of light.

2.3. X-ray diffraction

X-ray diffraction measurements were performed at room temperature in a Bruker AXS D5005 X-ray diffractometer, working with CuKα radiation (λ = 1.54184 Å), generated at 40 kV and 40 mA. Signal is recorded for 2θ between 20° and 85° with a step of 0.05°, a step time of 6 s and a rotation of 15 rpm.

2.4. Transmission electron microscopy

The pore structure was evaluated by transmission electron microscopy (TEM) in a Jeol 2100 UHR apparatus equipped with a LaB$_6$ filament with a 0.19 and 0.14 nm punctual and linear resolution, respectively. Energy dispersive X-ray (EDX) analysis was performed for local chemical analysis (in TEM mode). The X-ray emitted from the samples upon electron impact was collected in the 0–20 keV range.

Table 1
Characteristics of the supported gold catalysts.

Sample	Ce content in the support (wt.%)	Au content (wt.%)	S_{BET} (m^2 g^{-1}) Support/catalyst	Total OSC[a] (µmol O g^{-1})	OSC[b] (µmol O g^{-1})
Au/Al$_2$O$_3$	0	0.80	322/300	17	–
Au/Ce2Al	6.0	0.96	355/337	42	–
Au/Ce5Al	11.0	0.97	350/313	100	–
Au/Ce10Al	20.8	0.83	316/291	244	168
Au/Ce15Al	29.3	1.00	254/215	355	279
Au/Ce20Al	35.4	0.87	256/198	388	312
Au/CeO$_2$	80.7	0.98	222/232	225	149

[a] Total OSC values are based on the amount of CO$_2$ produced by the reduction of the catalyst with the first pulse of CO at 400 °C.
[b] Real OSC values are obtained considering the metal completely oxidized (Au$_2$O$_3$) before the first CO pulse and removing from total OSC values the contribution due to the reduction of the metal.

2.5. Temperature programmed reduction

Prior to the temperature programmed reduction (TPR) experiments, the catalyst (50 mg) was first pretreated in situ under oxygen at 400 °C for 30 min and cooled down to room temperature. After flushing under argon for 15 min, the reduction was carried out from room temperature up to 600 °C under a 1% H$_2$/Ar mixture, using a 5 °C min^{-1} as heating rate. The measurements of the hydrogen consumption were made in a AutoChem II/Micromeritics apparatus, using a thermal conductivity detector.

2.6. Oxygen storage capacity (OSC)

OSC measurements were carried out in an atmospheric glass fixed bed reactor placed in an electrical oven connected to a Porapak column and a TCD. The sample (6–8 mg) was placed into the reactor and heated up to 400 °C, 2 °C min^{-1}, under a continuous flow of helium (30 mL min^{-1}) at atmospheric pressure. At this temperature, 10 pulses (0.265 mL) of pure O$_2$ were introduced to oxidize completely the sample and a He flow was passed through the sample for 10 min to purge it. Then, 10 pure CO pulses were injected before a new purging step of 10 min with He. After 5 pulses of oxygen, the amount of oxygen immediately available (total OSC) is measured by alternating CO and O$_2$ pulses every 2 min.

2.7. Oxygen isotopic exchange

The oxygen isotopic exchange (OIE) reaction experiments were carried out in a closed-loop recirculating system coupled to a Pfeiffer Vacuum mass spectrometer. The complete isotopic exchange experimental set-up was already described in previous publications [36,37]. The solid samples (ca. 20 mg) were placed into a quartz U-form reactor and pre-treated prior to the experiment: the samples were oxidized under pure ^{16}O$_2$ flow (20 mL min^{-1}, 600 °C, 1 h) and evacuated for 1 h. After the pretreatment, the samples were cooled down to the reaction temperature.

For the Isothermal Oxygen Isotopic Exchange (IOIE) experiments, the reaction temperature was 550 °C. 65 mbar of pure ^{18}O$_2$ (≥99 at.%, ISOTEC) was introduced and initial level of $m/z = 36$ (^{18}O$_2$) was registered. The reaction of exchange was initiated at the opening of the reactor inlet and outlet where the total pressure diminished to 53 mbar and stayed constant during the duration of the experiment. The evolutions of each isotopomer concentration were analyzed by monitoring the following m/z: 32 (^{16}O$_2$), 34 (^{18}O^{16}O), and 36 (^{18}O$_2$). The 44, 46, 48, 28 m/z were also recorded in order to verify the absence of carbon dioxide and air in the system.

The calculation of the exchange rate (for isothermal experiment) was made based on the initial-rate method. In this method the tangent at the very beginning of the isotopomer concentrations versus time curve is used to determine the rate of the reaction. The final form of the isotopic exchange rate equation is the following:

$$r_e = -N_g \frac{d\alpha_g}{dt} \quad \text{with} \quad \frac{d\alpha_g}{dt} = \frac{1}{P_0}\left[2\frac{dP_{18_{O_2}}}{dt} + \frac{dP_{16_O18_O}}{dt}\right]$$

where N_g is the number of ^{18}O atoms in the gas phase at initial time; α_g is atomic fraction of ^{18}O in gas phase at time t, P_0 is total pressure, $P_{18_{O_2}}$ and $P_{16_O18_O}$ are the partial pressures of a ^{18}O$_2$ and ^{18}O^{16}O molecules, respectively.

An other important parameter, the number of exchanged atoms (N_e), is also used to compare the mobility of oxygen between the sample. It corresponds to the number of ^{18}O disappeared from the gas phase:

$$N_e = N_g(1 - \alpha_g)$$

2.8. Catalyst tests

Catalytic tests were performed at atmospheric pressure in a double wall glass reactor whose temperature was controlled by a Huber® thermocryostat. Because of the small size of the catalyst bed, it was assumed that there was no significant temperature profile in the system.

The standard CO-PrOx catalytic test mixture consisted of 2 vol.% CO, 2 vol.% O$_2$, 70 vol.% H$_2$, and He as a balance (the simple CO oxidation reactions were carried out under 2 vol.% CO, 2 vol.% O$_2$ and 96 vol.% He, at the same conditions), and the total inlet gas flow rate was fixed at 100 mL min^{-1}. All gases used were analytical grade (Alphagas-1) and were supplied by Air Liquide. Before each experiment the catalyst was pre-conditioned in situ at 160 °C, under 30 mL min^{-1} of O$_2$/He flowing (20 vol.%), heating rate 2 °C min^{-1}, for 30 min and then 10 min under He flow to purge the sample. Before starting the analyses at the highest temperature (160 °C), the catalyst is maintained 15 min under the reaction gas mixture.

In the experiments carried out by decreasing the temperature, three analysis of the gas at the reactor outlet were made at the same temperature, every 10 °C, with an interval of 4 min between each injection. Similar activity and selectivity values were obtained in each step. In these experiments, the mass of catalyst was fixed at 100 mg.

In the isothermal experiments at 100 °C, catalysts were submitted to the same above-mentioned pretreatment. After purging with He, the standard gas mixture was passed through the system for 15 min before starting the cooling down. After 15 min at stabilized temperature (100 °C), the first injection was made. In the first step, reaction was carried out for 5 h, with the same composition of the standard gas mixture, and injections were made every 15 min. After this time, 10 vol.% CO$_2$ was added to the feed and the reaction was performed for 1 h more (4 injections). Then, the standard gas mixture was again passed through the catalyst (2 injections,
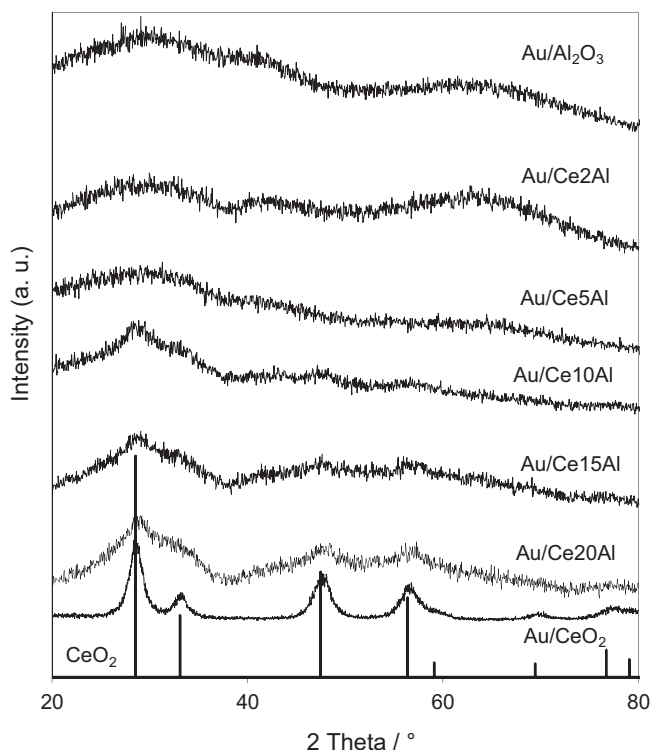
Fig. 1. XRD patterns of Au/Al_2O_3, Au/CeXAl and Au/CeO_2.

30 min), after 2 vol.% of H_2O was added to the standard feed, doing 4 injections (1 h), and finally the standard gas mixture was again passed through the catalyst (2 injections, 30 min). The mass of catalyst was fixed at 10 mg. All the catalysts were diluted in α-Al_2O_3 to obtain a total mass of 100 mg.

The gases were separated by a gas chromatograph (Varian® 3900) equipped with a Altech® CTR I column capable of separating H_2, O_2, CO_2, N_2, CH_4 and CO. Helium was used as the carrier gas. The oxygen and the carbon monoxide conversions were based on the oxygen and the carbon monoxide consumption, respectively:

$$X_{O_2} = \frac{F_{O_2}^{in} - F_{O_2}^{out}}{F_{O_2}^{in}} \times 100$$

$$X_{CO} = \frac{F_{CO}^{in} - F_{CO}^{out}}{F_{CO}^{in}} \times 100$$

where X is percentage of conversion and F is the (inlet or outlet) molar flow of the indicated gas. The selectivity is calculated by:

$$S_{CO_2} = \frac{F_{CO}^{in} - F_{CO}^{out}}{2 \times (F_{O_2}^{in} - F_{O_2}^{out})} \times 100$$

It represents the percentage of O_2 having reacted with CO. Carbon monoxide is exclusively converted to CO_2. Methane formation was not detected under our experimental conditions.

3. Results and discussion

3.1. Characterization

The main characteristics of the catalysts are reported in Table 1. The gold contents are close to the nominal value of 1 wt.%, whatever the support. No gold is identified on the X-ray diffractograms of the catalysts (Fig. 1), which are similar to those of the supports, demonstrating that the addition of gold does not change the

structure of the supports and that the gold content and/or particle size is too small to be detected. The synthesized supports are essentially amorphous. However, Au/Ce15Al and Au/Ce20Al present some diffraction peaks attributable to small crystallites of CeO_2. Au supported on the commercial ceria support presents a diffraction pattern characteristic of the cubic fluorite phase of ceria.

3.1.1. BET surface area

The Au/Al_2O_3 and Au/Ce(2,5,10)Al samples exhibit high BET surface areas, around $300 \, m^2 \, g^{-1}$, whereas the Au/CeO_2 and Au/Ce(15,20)Al samples present a smaller BET surface area, between roughly 200 and $230 \, m^2 \, g^{-1}$. The difference in the BET surface area observed for the gold supported catalysts is mainly due to the BET surface area of the supports, which is higher for alumina alone or with small amount of cerium (Ce(2,5,10)Al samples) than for the supports with more cerium. The change in the BET surface area due to the addition of gold can be considered as negligible for all the samples, except for the Au/Ce(15,20)Al samples for which the decrease in the BET surface area is higher than 15% compared to the support alone. This can be explained by a loss of organization with the incorporation of cerium, which may be accompanied with a decrease of the structural stability. The impregnation step of gold followed by a calcination step can slightly deteriorate the porosity and decrease the BET surface area. On the commercial support, certainly stabilized, the specific surface area is completely preserved.

3.1.2. Transmission electron microscopy

Fig. 2 shows examples of the TEM pictures obtained for all the catalysts. On the one hand, on the Au/Al_2O_3 and Au/Ce(2,5,10)Al samples (examples in Fig. 2a–e), small particles of gold, as well as large particles with diameters greater than 10 nm, were seen. No CeO_2 crystallites are visible on these TEM pictures. As no peak corresponding to gold was observed on the corresponding diffraction patterns, it can be inferred that these large particles are made up of many small crystallites. On the other hand, on the Au/Ce15Al and Au/Ce20Al samples (Fig. 2f–g), only small particles of gold with a maximum diameter of 2 nm are observed, demonstrating a better dispersion of gold on this kind of support. On the TEM images of the Au/CeO_2 catalyst (Fig. 2h), it is difficult to visualize the gold particles, due to the lack of contrast between gold and ceria. Concerning ceria in the Au/CeXAl, crystallographic planes related to ceria are clearly visible on the Au/Ce20Al sample (Fig. 2g), with very well dispersed crystallites with a diameter around 2 nm. EDX analyses on alumina aggregates showed homogeneous concentrations of cerium and gold in all samples and cerium is always associated with aluminum everywhere in the Au/CeXAl catalysts. Taking into account the XRD (Fig. 1) and TEM + EDX results, in the CeXAl supports, cerium is either in the form of small CeO_2 crystallites, or in a mixed structure with aluminum, and in both cases very well distributed in the alumina.

3.1.3. Temperature-programmed reduction

The TPR profiles of the catalysts, after pretreatment under oxygen at 300 °C, are shown in Fig. 2. No peak clearly appears during the reduction of Au/Al_2O_3. Then, it can be inferred that, even after the oxidizing pretreatment, gold is in a reduced state on this kind of support. It is known that autoreduction of gold easily occurs, even in non-reducing atmospheres. Thus, Grisel et al. [38] demonstrated that gold is mainly in the metallic state after calcination at 300 °C of their Au/Al_2O_3 catalyst prepared by deposition–precipitation by urea. When small amounts of cerium are added to alumina (Ce2Al and Ce5Al), small reduction peaks are observed on the TPR profiles indicating that, on the Au/Ce2Al and Au/Ce5Al catalysts, the amount of oxidized gold species remains negligible. For more important amounts of cerium in the support, two reduction peaks
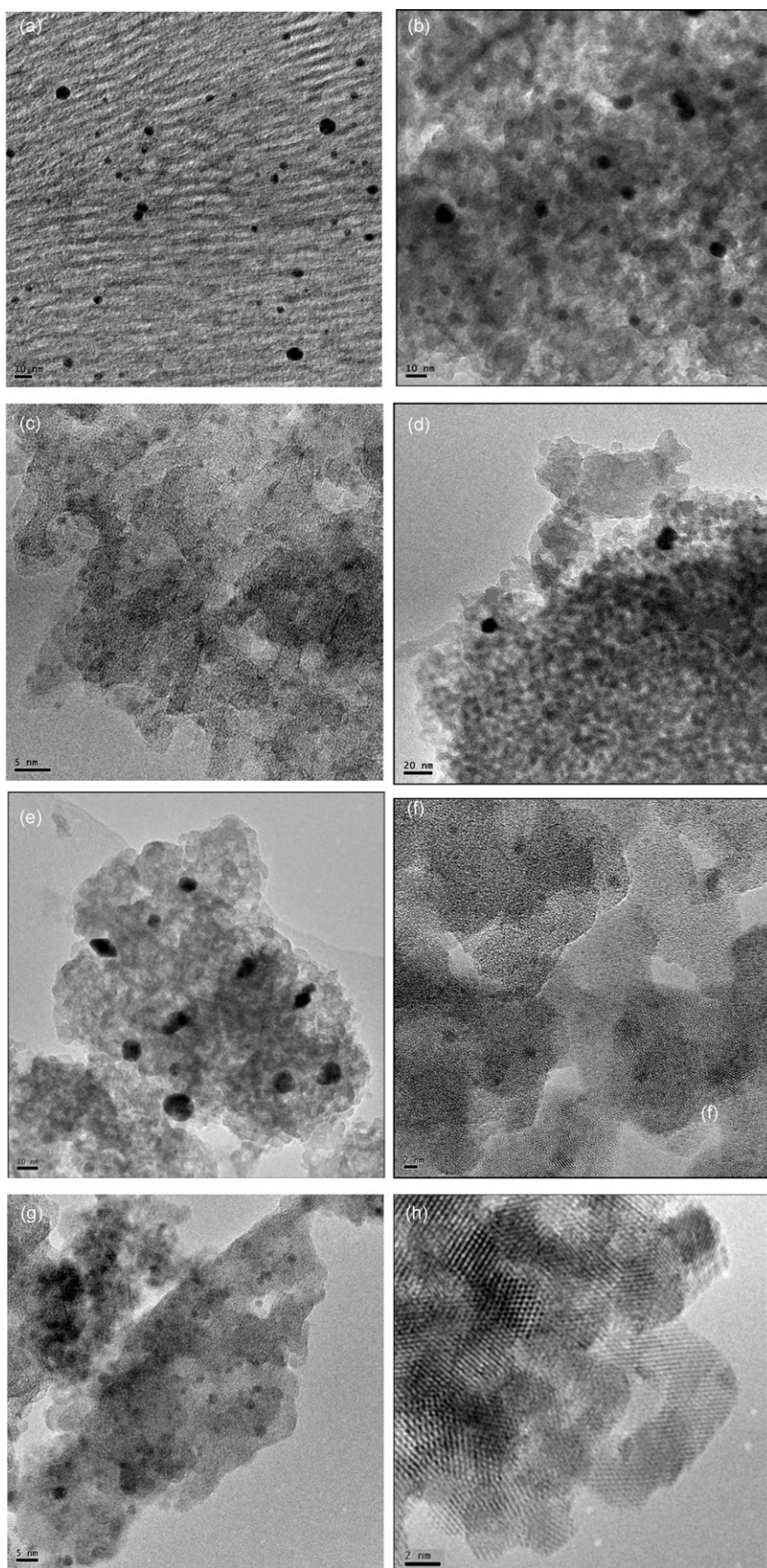
Fig. 2. TEM images: (a) Au/Al$_2$O$_3$; (b) Au/Ce2Al; (c) and (d) Au/Ce5Al; (e) Au/Ce10Al; (f) Au/Ce15Al; (g) Au/Ce20Al and (h) Au/CeO$_2$.
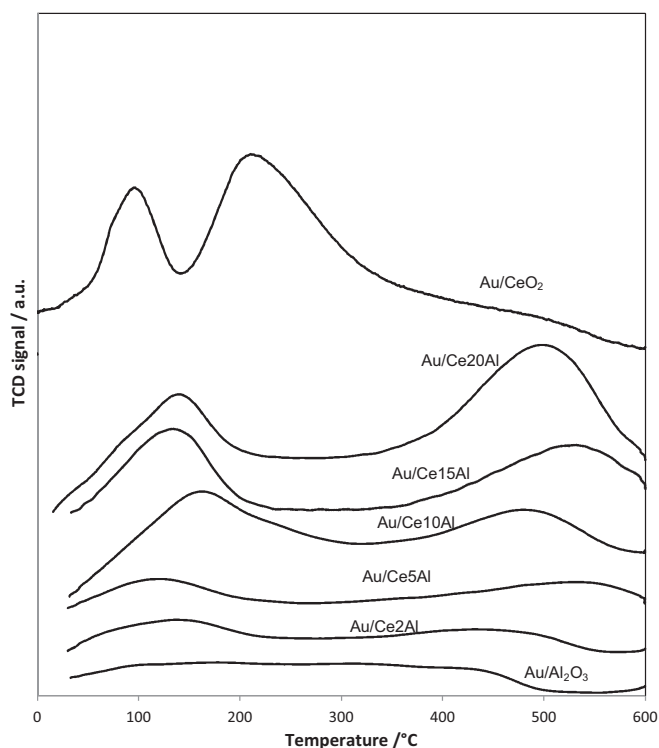
Fig. 3. Temperature-programmed reduction profiles of Au/Al$_2$O$_3$, Au/CeO$_2$ and Au/CeXAl catalysts.

are clearly seen on the TPR profiles of the catalysts. Their surface increases with the cerium content, whereas the temperature of the first peak decreases. Thus, the first peak is maximum at 163 °C for the Au/Ce10Al, at 140 °C for the Au/Ce20Al and 96 °C for Au/CeO$_2$. This first peak could be assigned in part to the reduction of oxygen species on the small gold particles. However, it was demonstrated on the Au/CeO$_2$ [28], for which this first peak is the most important of the series, that the H$_2$ consumption is higher than that necessary for a complete reduction of Au$_2$O$_3$ into Au^0. This result was explained by the reduction of a part of the ceria, at the interface of some gold nanoparticles at low temperature. The second peak, at higher temperature, from 212 °C for Au/CeO$_2$ up to 498 °C for Au/Ce20Al, may be attributed to the reduction of ceria [28,31]. Even if it is difficult to accurately quantify the H$_2$ consumption because of the difficulty of determining the baseline from the TPR profiles, one can see that the H$_2$ consumption on the Au/Ce20Al sample is similar to that of the Au/CeO$_2$ sample. It was demonstrated that the total H$_2$ consumption of the same Au/CeO$_2$ sample corresponded to the removal of 75% of the first layer of oxygen during the reduction process [28]. For the CeXAl oxides, it was deduced from the XRD and TEM + EDX results that cerium ions are well distributed in the alumina or in the form of small CeO$_2$ crystallites. If one considers that the oxygen atoms removed from the catalysts are necessarily linked to one cerium atom, it can be inferred from the comparison with the results obtained with gold on pure ceria that, in Au/CeXAl, and especially in the Au/Ce20Al sample, the reduction occurs also in the bulk. This is in accordance with the results of Andreeva et al. [31] who observed an enhancement of the bulk ceria reduction, due to an increase of the oxygen mobility, when alumina is added to ceria.

3.1.4. Oxygen storage capacity

The oxygen storage capacity (OSC) was determined at 400 °C on all the catalyst series in order to determine the amount of oxygen removed by reduction with CO to give CO$_2$. Fig. 3 presents the
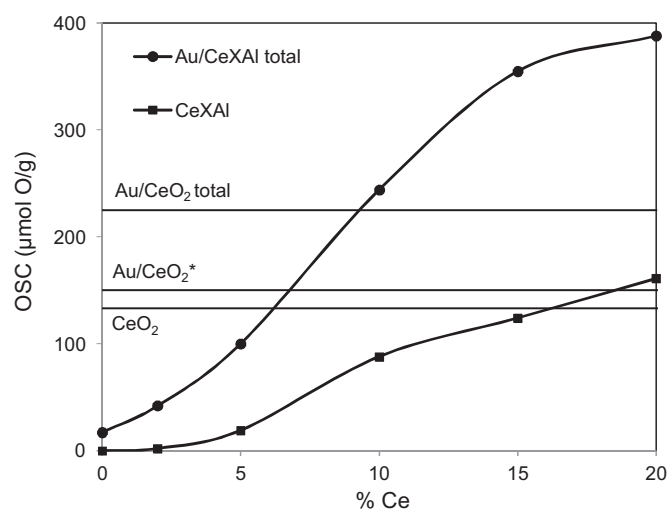

Fig. 4. Evolution of the oxygen storage capacity of the supports and Au supported-catalysts as a function of the cerium content. *Without gold reduction contribution.

evolution of the total OSC values as a function of the cerium content in the support, for the supports alone and for the gold supported catalysts. For reference, the OSC values of the CeO$_2$ support with or without gold are also presented in this figure by a horizontal line. The OSC values are summarized in Table 1. The total OSC values are given, which do not take into account the possibility of CO consumption by gold (Au^{3+} → Au^0 reduction), as well as the real OSC for Au/CeXAl with $X \geq 10$, calculated by removing the reduction of gold, since it was shown by TPR that the reduction of gold may occur at temperatures lower than 200 °C for these catalysts. The complete reduction of Au$_2$O$_3$ (1 wt.% of Au) would contribute to 76 μmol O g^{-1} for all the OSC values.

Fig. 4 shows that for the supports alone, the OSC value for the Ce15Al approaches that of pure ceria and the value of Ce20Al is slightly superior to the latter. When gold is added to the support, there is a significant enhancement of the oxygen storage capacity for Ce10Al, Ce15Al and Ce20Al, compared to the supports alone, which is not the case for the Au/CeO$_2$ (Fig. 4) and for the Au/Al$_2$O$_3$ catalysts. Moreover values reported in Table 1 show that the OSC values of Au/Ce($X \geq 10$)Al are much higher than that of the Au/CeO$_2$ catalyst. Whereas the total OSC value of Au/CeO$_2$ is of 225 μmol O g^{-1} (149 μmol O g^{-1} if the contribution of gold is removed), the value for Au/Ce($X \geq 10$)Al catalysts, is much higher, from 244 for Au/Ce10Al to 388 μmol O g^{-1} for Au/Ce20Al. This result shows that the ability of the Au/Ce($X \geq 10$)Al oxides to be reduced during the process is much higher than that of pure ceria. The presence of gold strongly facilitates the reduction of the CeXAl support, which may be attributed the CO adsorption on the metal and subsequent reaction at the Au–CeXAl interface. The small size of ceria crystallites in the CeXAl as well as the defective structure due to the presence of alumina may explain the enhanced reducibility, and then oxygen mobility, of this kind of catalyst.

3.1.5. Isothermal oxygen isotopic exchange (IOIE)

IOIE experiments were performed on Au/Al$_2$O$_3$, Au/Ce(2,10,20)Al and Au/CeO$_2$. In order to highlight the effect of the gold nanoparticles, bare supports were also studied. The evolutions of the number of oxygen atoms exchanged in gold catalysts (N_e) are reported in Fig. 5 as a function of time. A comparison of the N_e values calculated after 1 h IOIE reaction is given in Table 2. One can see that the mobility of oxygen in Au/Al$_2$O$_3$ is not very important since after 1 h exchange, the number of exchanged atoms in this sample remains low. However, it should be noticed that on bare alumina, N_e is almost nil even after 1 h (curve not showed) showing
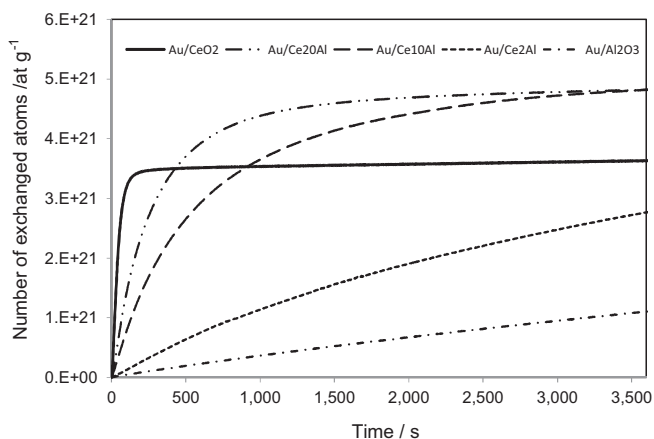
Fig. 5. Evolution of the number of exchanged oxygen atoms in the catalysts as a function of time obtained at 550 °C.

that gold presence improves the oxygen exchange. Increasing the cerium content in the samples leads to a significant increase in the mobility of oxygen atoms. Even a small incorporation of Ce in the sample (Ce2Al) enables to multiply the N_e value by a factor of 2.5. This improvement cannot be explained by the exclusive exchange of ceria oxygen atoms. When the molar percentage of Ce became superior to 10, the number of oxygen atoms exchanged achieves the value that corresponds to the equilibrium between the ^{18}O concentration in the gas phase and the ^{18}O concentration in the solid. This value, which is 4.82×10^{21} at. g^{-1} for Au/Ce10Al and Au/Ce20Al, is superior to the value obtained for Au supported on pure ceria (3.63×10^{21} at. g^{-1}). Taking into account that the experiments were performed using the same mass and the same $^{18}O_2$ initial pressure, such a result indicates that surprisingly the number of exchangeable atom in CeAl sample is higher than in CeO$_2$. These results are in accordance with the OSC results, which have demonstrated better oxygen mobility in this type of support.

At initial time we determined the rate of exchange (r_e) for each catalyst: the corresponding values are reported in Table 2 and compared with the r_e values obtained on bare supports. Based on the initial rate of oxygen exchange, the following ranking can be proposed: Au/CeO$_2$ > Au/Ce20Al > Au/Ce10Al Au/Ce2Al > Au/Al$_2$O$_3$. Moreover, looking at the r_e values of the bare support, it clearly confirms that both the presence of Au nanoparticles and the increase of Ce content participate to the improvement of the oxygen mobility. The evolutions of the $^{16}O_2$ ($m/z = 32$) and $^{18}O^{16}O$ ($m/z = 34$) partial pressures as a function of time give us crucial information on the possible reasons which could explain this improvement. A comparison of the corresponding curves between the Ce10Al, Ce20Al, CeO$_2$ bare supports and the Au supported samples is presented in Fig. 6. At the beginning of the exchange reaction, on the support, the two $^{18}O^{16}O$ and $^{16}O_2$ isotopomers are formed simultaneously. It is a well known phenomenon for ceria since it was already reported

Table 2
Initial rate of exchange and number of atoms exchanged obtained from isothermal oxygen isotopic exchange experiments over the supported gold catalysts at 550 °C.

Sample	r_e ($\times 10^{18}$ at. g^{-1} s^{-1})	N_e [b] ($\times 10^{21}$ at. g^{-1})
Au/Al$_2$O$_3$	0.36 (n.s.)[a]	1.11
Au/Ce2Al	1.54 (0.36)	2.77
Au/Ce10Al	8.16 (1.83)	4.82
Au/Ce20Al	12.20 (4.95)	4.82
Au/CeO$_2$	49.00 (22.90)	3.63

[a] Values between parentheses were obtained over bare oxide without gold. n.s.: not significant.
[b] Number of oxygen atoms exchanged after 1 h of reaction, at 550 °C, during the ^{18}O isotopic oxygen exchange.

that this oxide exchanges oxygen via the two types of mechanism [39,40]: the simple exchange which produces $^{18}O^{16}O$ and the multiple or complex exchange which directly gives $^{16}O_2$. The presence of gold makes the $^{16}O_2$ isotopomer majoritory and thus favors the multiple exchange. Taking into account that the multiple exchange should involve binuclear oxygen species as intermediate, we can conclude that the interaction between the gold nanoparticles and the ceria crystallites is the location of defect centers where oxygen is activated in the form of peroxide or superoxide species as suggested by Winter to explain the complex exchange mechanism observed over basic oxides [41]. Corma et al. described on gold supported on nanocrystalline CeO$_2$ spectroscopic evidences to correlate surface oxygen species and CO oxidation activity [42]. The authors reported that superoxide species and peroxide adspecies at the one-electron defect site are the active species in the catalytic reaction. The peroxide adspecies would be formed near a cationic Au stabilized by Ce^{3+} and oxygen vacancy sites.

Furthermore, the interaction between ceria and alumina in the CeAl oxide support allows the involving of the oxygen of alumina in the exchange at a temperature where they are not involved in alumina alone.

3.2. Catalytic tests

3.2.1. Total CO oxidation

CO oxidation was studied by decreasing the temperature from 160 °C to RT, after a pretreatment under diluted oxygen before introducing the reaction gas mixture, containing 2% of CO and 2% of O$_2$, i.e. an excess of oxygen. Results obtained in CO oxidation are reported in Fig. 7. One can see that the activity of Au/Al$_2$O$_3$ is very low, with a negligible CO conversion at high temperature. On this kind of catalyst, it was proposed [17] that the oxygen adsorption and dissociation may only occur directly on small metallic gold nanoparticles, facilitated by the change in the electronic structure at decreasing size [43,44] or by the presence of more defect sites (steps, edges and kinks) [45,46]. It has also been suggested that the active sites for CO oxidation over Au/Al$_2$O$_3$ involve an ensemble of metallic Au atoms and Au(I) cations with hydroxyl ligands [47,50]. After the pretreatment at 160 °C under diluted oxygen, the hydroxyl groups are likely to be removed leading to a deactivation of the catalyst. Then, the low activity may be explained on the one hand by the low dispersion of gold on the alumina support, a large amount of particles presenting sizes higher than 10 nm, as observed by TEM, and on the other hand by the absence of active oxygen and/or gold species in the reaction conditions. For Au/CeAl catalyst, reactive oxygen species may be provided by the support, via a Mars and van Krevelen mechanism, and may react more easily with CO adsorbed on gold particles at the metal–support interface, decreasing the dependence of the reaction rate on the gold particle diameter [17]. Thus, the activity increases with the cerium content of the support, in accordance with the results reported in Ref. [51]. However, the complete CO conversion is not reached for Au/Ce(2,5)Al at 160 °C. The most active catalyst is Au/CeO$_2$, which is able to completely convert CO at 50 °C. There is a good correlation between the catalytic activity and the oxygen storage capacity, in agreement with the results of [30], except for Au/CeO$_2$, which is the most active catalyst for CO oxidation with an intermediate OSC value, between those of Au/Ce5Al and Au/Ce10Al. However, even if the Au/CeO$_2$ catalyst shows a lower OSC value that some Au/CeAl samples, on this catalyst all the gold nanoparticles are well dispersed on ceria and consequently the gold–ceria interface is higher than on the Au/CeAl catalysts, for which the support contains less than 20% of cerium compared to aluminum. Even if the temperature ranges studied are different, the correlation between the CO oxidation activity and the rate of exchange is clearer since the same ranking is obtained in both series of experiment. It
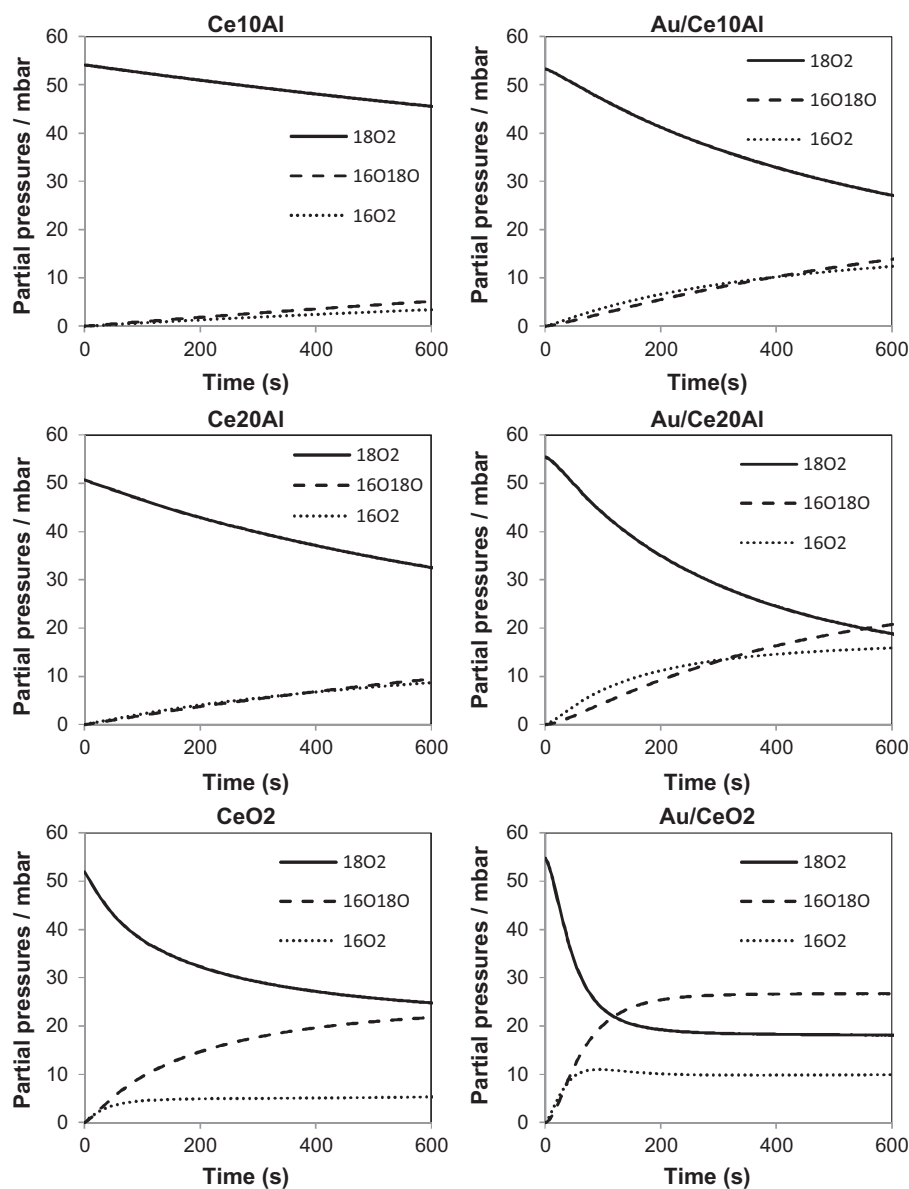
Fig. 6. Impact of the gold nanoparticles on the evolutions of each isotopomer partial pressure registered during the oxygen isotopic exchange experiment performed at 550 °C on Ce10Al, Ce20Al and CeO$_2$.

reinforces the hypothesis that in CO oxidation reaction the gold/ceria interface is the place where oxygen could be activated and reacts easily with activated CO and it suggests that the reactional area could be enlarged by a strong mobility of the support.

3.2.2. Preferential CO oxidation

Preferential CO oxidation was performed in the same experimental conditions as those used for total CO oxidation but in the presence of a large amount of hydrogen (70%), by decreasing the temperature from 160 °C, after a pretreatment under diluted oxygen. Fig. 8a–c shows the O$_2$ and CO conversion and the selectivity to CO$_2$, respectively, as a function of temperature for the Au/Al$_2$O$_3$, Au/Ce(2,5,10,20)Al and Au/CeO$_2$. Depending on the catalyst, the O$_2$ conversion is complete from 70 °C, for Au/Ce10Al, to 100 °C, for Au/Al$_2$O$_3$ (Fig. 8a). As the amount of oxygen at the inlet is of 2 vol.% and only 1% is needed to convert all the CO (2 vol.%), this means that 1% of the oxygen has reacted with hydrogen to produce water. Consequently, the thermodynamics of water-gas shift (WGS) and reverse (RWGS) was used to calculate the conversion of CO from
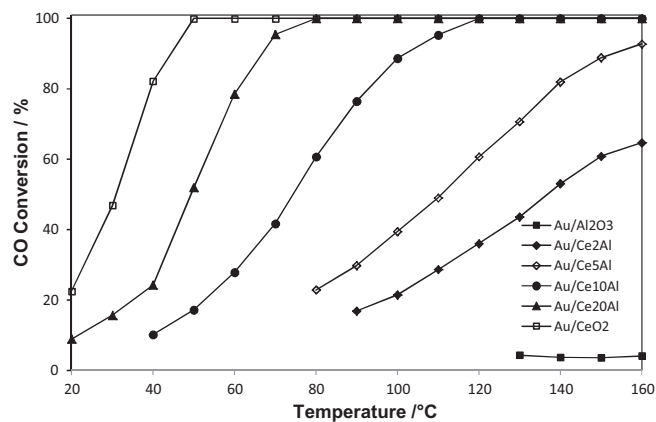

Fig. 7. Evolution of CO conversion versus temperature obtained during the simple CO oxidation reaction. Experimental conditions: 2% CO, 2% O$_2$, 96% He, 100 mg of catalyst, total gas inlet: 100 mL min^{-1}.

Table 3

Maximum CO conversion, CO conversion at 60 °C, and corresponding temperatures and CO_2 selectivities during the CO-PrOx reaction in the presence of supported gold catalysts (experimental conditions: 2% CO, 2% O_2, 70% H_2, 26% He, 100 mg of catalyst, total gas inlet: 100 mL min^{-1}).

	Au/Al_2O_3	Au/Ce2Al	Au/Ce5Al	Au/Ce10Al	Au/Ce20Al	Au/CeO_2
Max CO conversion (%)	85	97	100	99	91	98
CO concentration at the outlet (ppm)	3000	600	0	200	1800	400
Rate of CO conversion (mmol s^{-1} g$_{Au}$$^{-1}$)	1.58	1.50	1.53	1.77	1.55	1.49
T^a (°C)	70	60	60	50	60	90
S_{CO_2}^{a} (%)	52	52	54	63	49	49
CO conversion (%) at 60 °C	79	97	100	99	91	83
S_{CO_2}^{b} (%)	67	52	54	51	49	55

^{a} At maximum of CO conversion.

^{b} At 60 °C (temperature of fuel cell operation).

70 °C at the thermodynamic equilibrium [28,52]. The values are reported in Fig. 8b. As far as the experimental data of CO conversion are concerned (Fig. 8b), it can be seen that at low temperature, lower than 60 °C, the highest CO conversion is obtained with gold supported on Ce–Al oxides, Au/Al_2O_3 and Au/CeO_2 being less active with similar conversions. Among the Au/CeXAl, the Au/Ce20Al is the less active catalyst. When the temperature is higher, the CO conversion decreases, except for the Au/CeO_2 sample, which presents a stable CO conversion, between 94 and 98% from 80 °C to 160 °C. The decrease in activity at higher temperature is due to both a competition between H_2 and CO oxidation on the same site and the lack of oxygen in the feed limiting the reaction [15,53–55]. For the Au/CeO_2 sample, the evolution of CO conversion versus the temperature fits to that calculated at the thermodynamic equilibrium of the WGS/RWGS reaction. This result may be explained by the high activity of the Au/CeO_2 catalyst for the water-gas shift (WGS) reaction, allowing the production of CO_2 and H_2 from CO and water [56,57], produced by oxidation of hydrogen. As far as the selectivity is concerned, the evolution as a function of temperature can be considered as similar whatever the catalyst, with a decrease in the selectivity when the temperature increases. However, at the highest temperature, the selectivity of the Au/CeO_2 catalyst is slightly less affected, which is in accordance with the possibility of converting CO into CO_2 by the WGS reaction. The results are summarized in Table 3, which reports the highest CO conversion, the amount of CO at the outlet, the reaction rate and the corresponding temperature and CO_2 selectivity, as well as the CO conversion and CO_2 selectivity at 60 °C (fuel cell operating temperature). One can see that the Au/Ce5Al and Au/Ce10Al are the most active catalysts. At 60 °C, they present a similar CO conversion (99–100%) and CO_2 selectivity (51–54%). However, at 50 °C, the Au/Ce10Al is more interesting, with 99% of CO conversion and 63% of CO_2 selectivity. For comparison with the results of the literature obtained in similar conditions are reported in Table 4. Rossignol et al. [58] obtained at maximum 85% of CO conversion at 100 °C with a selectivity to

CO_2 of roughly 50% with 1.47 wt.% Au/TiO_2, Avgouropoulos et al. [23] reached 96% of CO conversion with 3% Au/CeO_2 at 90 °C with a selectivity of 39%. More recently, Ivanova et al. [57] also obtained a maximum of CO conversion of 96% but at 135 °C on 1.95% Au/CeO_2. To summarize, at low temperature, 50–60 °C, gold supported on Ce–Al oxides are more active than when supported on the CeO_2 or Al_2O_3 and the best catalysts are the ones containing a medium Ce/Al ratio. However, our Au/CeO_2 catalyst presents interesting performances in CO-PrOx compared to the Au/CeO_2 catalysts of the literature.

Now, if one compares the performances in total CO oxidation and in preferential CO oxidation, one can see that, at low temperature, the CO conversion is higher in the PrOx conditions than in absence of H_2 for all the catalysts, except Au/CeO_2. The effect is more pronounced for the Au/Al_2O_3 catalyst, which has shown a negligible activity in CO oxidation in the absence of H_2, and the difference in activity between the CO-PrOx and the CO oxidation decreases when the amount of cerium in the support increases. The positive effect on the gold catalysts supported on alumina containing supports is explained in the literature [48–50,59] by the formation of H_2O by H_2 oxidation regenerating the active sites involving hydroxyl groups. As this promoting effect is also effective from room temperature, when H_2 oxidation is not possible, other authors [54,58] proposed mechanisms in which hydrogen may react with molecular oxygen, associatively adsorbed [54] or in the gas phase [58] to produce surface intermediates able to oxidize CO into CO_2. The Au/CeO_2 catalyst shows an opposite behavior, since it is more active in CO oxidation than in CO-PrOx: in the absence of hydrogen, 100% of CO conversion is reached at 50 °C, whereas in the PrOx conditions, the maximum of CO conversion, 98% is obtained at 90 °C. This behavior has already been reported for gold supported on reducible supports such as CeO_2 [30] and on other active supports [53] and was explained by the blocking effect of H_2O on the anionic vacancies necessary for the Mars–van Krevelen mechanism. However, it was demonstrated that moisture

Table 4

Comparison of catalytic performances of gold catalysts in CO-PrOx reaction in similar conditions.

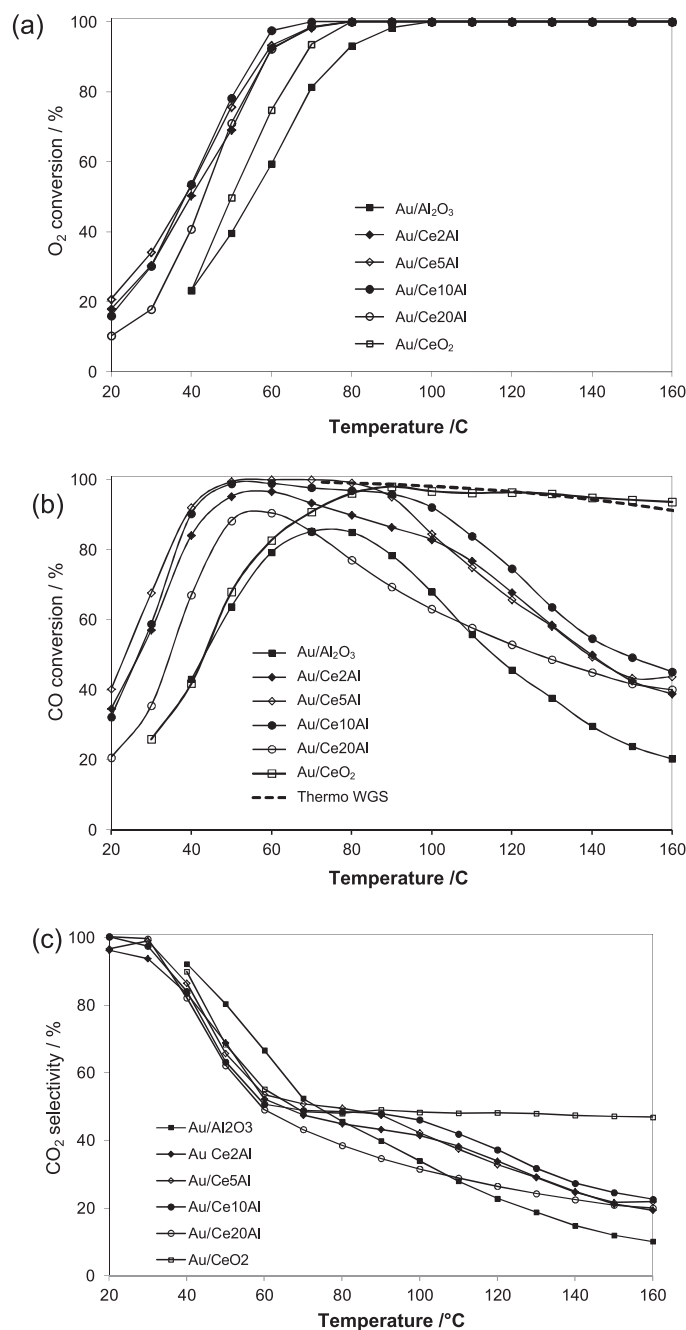| Catalyst	Feed	W/F (g$_{Au}$ s cm^{-3})	Temperature of maximum CO conversion (°C)	Maximum CO conversion (%)	Activity at maximum CO conversion (mmol g$_{Au}$$^{-1}$ s^{-1})	Selectivity to CO_2 (%)	Ref.
0.83% Au/Ce10Al	2% CO 2% O_2 70% H_2	5×10^{-4}	50	99%	1.77	63	Present study
3% Au/CeO_2	1% CO 1.25% O_2 50% H_2	9×10^{-4}	90	96	0.476	39	[23]
1.47% Au/TiO_2	2% CO 2% O_2 48% H_2	2×10^{-4}	100	85	3.72	50	[58]
1.95% Au/TiO_2	2% CO 2% O_2 48% H_2	2×10^{-4}	135	96	4.2	55	[57]

Fig. 8. Evolution of O_2 (a) and CO (b) conversions and selectivity in CO_2 (c) versus temperature obtained during the CO-PrOx reaction. Experimental conditions: 2% CO, 2% O_2, 70% H_2, 26% He, 100 mg of catalyst, total gas inlet: 100 mL min^{-1}.

Fig. 9. Evolution of CO conversion (a) and selectivity in CO_2 (b) versus time obtained during the CO-PrOx reaction. Experimental conditions: 2% CO, 2% O_2, 70% H_2, 26% He, T = 100 °C, 10 mg of catalyst, total gas inlet: 100 mL min^{-1}.

has a promoting effect on CO oxidation (1% CO, 0.5% C_6H_6, 3% H_2O, in air) [60], using an Au/CeO_2 catalyst under oxidizing conditions. In the present study, CO oxidation is performed with an excess of oxygen (2% of CO, 2% of O_2, 96% He), i.e. in a globally oxidizing atmosphere. Thus, the ceria surface is globally oxidized and active oxygen species are easily provided at the support–metal interface to react with CO. In CO-PrOx conditions (2% CO, 2% O_2, 70 H_2, and He as a balance), the reaction is performed under reducing conditions. Remembering that the reaction was started from 160 °C and performed by decreasing the temperature, surface ceria is partially reduced. Consequently, oxygen is activated not only at the gold–ceria interface but also on the ceria surface, far from the gold particles where CO is adsorbed. Another explanation on the negative effect of H_2 on CO oxidation in the presence of Au/CeO_2 may
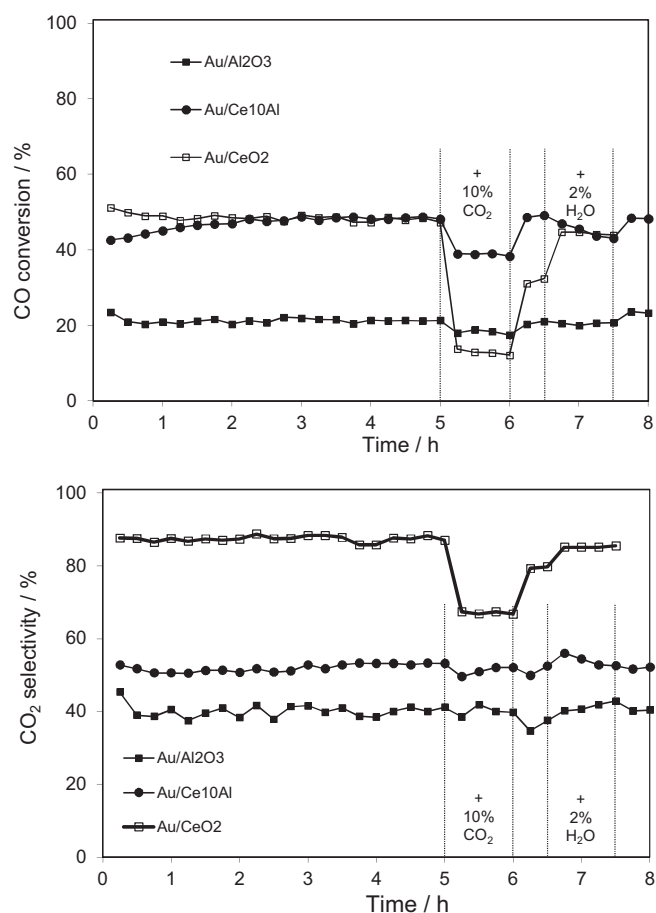
be the formation of stable intermediate species, such as carbonates, blocking ceria surface sites.

The stability of three catalysts of the series, namely Au/Al_2O_3, Au/Ce10Al and Au/CeO_2 was evaluated at 100 °C during 8 h in the CO-PrOx conditions. CO_2 and H_2O were alternatively introduced after 5 h and 6 h 30 min of time-on-stream, respectively. Results in terms of CO conversion and selectivity in CO_2 are reported in Fig. 9a and b. All the catalysts evaluated are stable in CO-PrOx conditions during the first 5 h of time on stream in the absence of carbon dioxide and water. One can see that Au/CeO_2 and Au/Ce10Al present a similar activity with a CO conversion around 50% (Fig. 9a). When CO_2 is introduced in the gas stream, these catalysts deactivate and the deactivation increases with the cerium content. Schubert et al. [16] explained this deactivation by a competitive adsorption of CO_2 on the gold surface or at the gold–support interface, and to an increased formation of deactivating carbonates. The increase of the cerium content leads to an increase of the basicity of the support and thus an easier carbonate formation at the interface. On the Au/CeO_2 catalyst, the presence of CO_2 only affects the CO conversion, and not the H_2 conversion, since the selectivity into CO_2 is decreased (Fig. 8b). On Au/Ce10Al, the presence of CO_2 has no important effect on the selectivity. Since CO conversion was decreased by the addition of CO_2, it can be inferred that, on this Au/Ce10Al catalyst, H_2 oxidation is decreased in a same extent. When CO_2 is removed from the gas phase, the Au/Ce10Al catalyst recovers its initial CO conversion, which is not the case for the Au/CeO_2 catalysts, which is partially reactivated. As far as the Au/Al_2O_3 catalyst is concerned, it presents lower CO conversion

and CO_2 selectivity than the two other catalysts, with roughly 20% of CO conversion and 40% of CO_2 selectivity. However, the addition of CO_2 in the gas stream does not modify its performances. At last, steam has no sensitive effect on the catalytic performances, whatever the catalyst. Steam very slightly deactivates the Au/Ce10Al sample, whereas the Au/CeO$_2$ recovers its initial activity. This result confirms that the lower activity of the Au/CeO$_2$ catalyst in CO-PrOx than in CO oxidation cannot be explained by water formation from H_2 oxidation.

4. Conclusion

Gold supported on aluminum–cerium oxides (Ce/Ce + Al = 0, 2, 5, 10, 15 and 20 mol%) and on commercial pure ceria were characterized and tested in CO oxidation, in the absence and in the presence of hydrogen (CO-PrOx) conditions. The reducibility of the supports during TPR and OSC is enhanced by the presence of gold and globally increases with the cerium content, as well as the oxygen mobility. The Au/CeXAl with high cerium contents show particular behavior, with higher OSC values than Au/CeO$_2$, due to the small size of ceria crystallites in the CeXAl as well as the defective structure due to the presence of alumina. The activity in CO oxidation increases with the cerium content in the support, globally following the same trend as that evidenced by TPR, OSC, and isotopic exchange, whereas in CO-PrOx the gold catalysts supported on Ce–Al oxides with medium cerium contents present the highest CO conversion at 50–60 °C. The catalysts are stable at 100 °C in CO + O$_2$ + H$_2$ mixtures. The addition of CO_2 in the stream strongly deactivates Au/CeO$_2$, whereas Au/Ce10Al is less affected. Whatever the catalyst, the presence of steam has no significant effect on the catalytic performances.

Acknowledgments

References

[1] G.J.K. Acres, J.C. Frost, G.A. Hards, R.J. Potter, T.R. Ralph, D. Thompsett, G.T. Burstein, G.J. Hutchings, Catalysis Today 38 (1997) 393–400.
[2] B. Rohland, V. Plzak, Journal of Power Sources 84 (1999) 183–186.
[3] J. Harger, H. Terrey, U.S.P. 1366176 (1921).
[4] E.K. Rideal, H.S. Taylor, U.S.P. 1375932 (1921).
[5] M. Haruta, N. Yamada, T. Kobayashi, S. Iijima, Journal of Catalysis 115 (1989) 301–309.
[6] M. Haruta, T. Tsubota, T. Kobayashi, H. Kageyama, M.J. Genet, B. Delmon, Journal of Catalysis 144 (1993) 175–192.
[7] M. Haruta, Catalysis Today 36 (1997) 153–166.
[8] N. Bion, F. Epron, M. Moreno, F. Mariño, D. Duprez, Topics in Catalysis 51 (2008) 76–88.
[9] E.D. Park, D. Lee, H.C. Lee, Catalysis Today 139 (2009) 280–290.
[10] M. Haruta, Cattech 6 (2002) 102–115.
[11] G.C. Bond, C. Louis, D.T. Thompson, Catalysis by Gold, Imperial College Press, London, 2006, p. 161.
[12] T.V.W. Janssens, B.S. Clausen, B. Hvolbæk, H. Falsig, C.H. Christensen, T. Bligaard, J.K. Nørskov, Topics in Catalysis 44 (2007) 15–26.
[13] J.J. Delgado, J.M. Cíes, M. López-Haro, E. del Río, J.J. Calvino, S. Bernal, Chemistry Letters 40 (2011) 1210–1216.
[14] C. Galetti, S. Fiorot, S. Specchia, G. Saracco, V. Specchia, Chemical Engineering Journal 134 (2007) 45–50.
[15] B. Schumacher, Y. Denkwitz, V. Plzak, M. Kinne, Journal of Catalysis 224 (2004) 449–462.
[16] M. Schubert, A. Venugopal, M. Kahlich, V. Plzak, R. Behm, Journal of Catalysis 222 (2004) 32–40.
[17] M.M. Schubert, S. Hackenberg, A. van Veen, M. Muhler, V. Plzak, R.J. Behm, Journal of Catalysis 197 (2001) 113–122.
[18] R.M. Torres Sanchez, A. Ueda, K. Tanaka, M. Haruta, Journal of Catalysis 168 (1997) 125–127.
[19] A. Luengnaruemitchai, D.T.K. Thoa, S. Osuwan, E. Gulari, International Journal of Hydrogen Energy 30 (2005) 981–987.
[20] A. Luengnaruemitchai, S. Osuwan, E. Gulari, International Journal of Hydrogen Energy 29 (2004) 429–435.
[21] F. Moreau, G.C. Bond, Catalysis Today 114 (2006) 362–368.
[22] F. Arena, P. Famulari, G. Trunfio, G. Bonura, F. Frusteri, L. Spadaro, Applied Catalysis B: Environmental 66 (2006) 81–91.
[23] G. Avgouropoulos, J. Papavasiliou, T. Tabakova, V. Idakiev, T. Ioannides, Chemical Engineering Journal 124 (2006) 41–45.
[24] G. Avgouropoulos, J. Papavasiliou, T. Ioannides, Catalysis Communications 9 (2008) 1656–1660.
[25] W. Deng, J. de Jesus, H. Saltsburg, M. Flytzani-Stephanopoulos, Applied Catalysis A-General 291 (2005) 126–135.
[26] A. Jain, X. Zhao, S. Kjergaard, S.M. Stagg-Williams, Catalysis Letters 104 (2005) 191–197.
[27] E.-Y. Ko, E. Duck Park, K.W. Seo, H.C. Lee, D. Lee, S. Kim, Catalysis Today 116 (2006) 377–383.
[28] J.S.L. Fonseca, H.S. Ferreira, N. Bion, L. Pirault-Roy, M.C. Rangel, D. Duprez, F. Epron, Catalysis Today 180 (2012) 34–41.
[29] T. Tabakova, F. Boccuzzi, M. Manzini, D. Andreeva, Applied Catalysis A 252 (2003) 385–397.
[30] S. Carettin, P. Concepción, A. Corma, J.M. López Nieto, V.F. Puntes, Angewandte Chemie International Edition 43 (2004) 2538–2540.
[31] D. Andreeva, I. Ivanov, L. Ilieva, M.V. Abrashev, Applied Catalysis A-General 302 (2006) 127–132.
[32] R. Ramírez-López, I. Elizalde-Martinez, L. Balderas-Tapia, Catalysis Today 150 (2010) 358–362.
[33] M. Aresta, A. Dibenedetto, C. Pastore, A. Angelini, B. Aresta, I. Pápai, Journal of Catalysis 269 (2010) 44–52.
[34] Q. Yuan, H.-H. Duan, L.-L. Li, Z.-X. Li, W.-T. Duan, L.-S. Zhang, W.-G. Song, C.-H. Yan, Advanced Materials 22 (2010) 1475–1478.
[35] Q. Yuan, A.-X. Yin, C. Luo, L.-D. Sun, Y.-W. Zhang, W.-T. Duan, H.-C. Liu, C.-H. Yan, Journal of the American Chemical Society 130 (2008) 3465–3472.
[36] D. Martin, D. Duprez, Journal of Physical Chemistry 100 (1996) 9429–9438.
[37] S. Ojala, N. Bion, S. Rijo Gomes, R. Keiski, D. Duprez, ChemCatChem 2 (2010) 527–533.
[38] R.J.H. Grisel, C.J. Weststrate, A. Goosens, M.W.J. Crajé, A.M. van des Kraan, B.E. Nieuwenhuys, Catalysis Today 72 (2002) 123–132.
[39] Y. Madier, C. Descorme, A.M. Le Govic, D. Duprez, Journal of Physical Chemistry B 103 (1999) 10999–11006.
[40] D. Duprez, in: J.S. Hargreaves, S.D. Jackson, G. Webb (Eds.), Isotopes in Catalysis, Catalytic Science Series, vol. 4, Imperial College Press, 2006, pp. 133–181.
[41] E.R.S. Winter, Journal of the Chemical Society A (1968) 2889–2902.
[42] J. Guzman, S. Carretin, A. Corma, Journal of the American Chemical Society 127 (10) (2005) 3286–3287.
[43] D.A.H. Cunningham, W. Vogel, H. Kageyama, S. Tsubota, M. Haruta, Journal of Catalysis 177 (1998) 1–10.
[44] M. Valden, S. Paka, X. Lai, D.W. Goodman, Catalysis Letters 56 (1998) 7–10.
[45] M. Mavrikakis, P. Stoltze, J.K. Nørskov, Catalysis Letters 64 (2000) 101–106.
[46] J.-D. Grunwaldt, M. Maciejewski, O.S. Becker, P. Fabrizioli, A. Baiker, Journal of Catalysis 186 (1999) 458–469.
[47] G.C. Bond, D.T. Thompson, Gold Bulletin 33 (2000) 41–50.
[48] C.K. Costello, M.C. Kung, H.S. Oh, Y. Wang, H.H. Kung, Applied Catalysis A-General 232 (2002) 159–168.
[49] C.K. Costello, J.H. Yang, H.Y. Law, Y. Wang, J.-N. Lin, L.D. Marks, M.C. Kung, H.H. Kung, Applied Catalysis A-General 243 (2003) 15–24.
[50] H.H. Kung, M.C. Kung, C.K. Costello, Journal of Catalysis 216 (2003) 425–432.
[51] P. Lakshmanan, L. Delannoy, V. Richard, C. Métivier, C. Potvin, C. Louis, Applied Catalysis B: Environmental 96 (2010) 117–125.
[52] D. Tibiletti, E.A. Bart de Graaf, S. Pheng Teh, G. Rothenberg, D. Farusseng, C. Mirodatos, Journal of Catalysis 225 (2004) 489–497.
[53] R.J.H. Grisel, B.E. Nieuwenhuys, Journal of Catalysis 199 (2001) 48–59.
[54] E. Quinet, F. Morfin, F. Diehl, P. Avenier, V. Caps, J.-L. Rousset, Applied Catalysis B: Environmental 80 (2008) 195–201.
[55] M.J. Kahlich, H.A. Gasteiger, R.J. Behm, Journal of Catalysis 182 (1999) 430–440.
[56] R. Burch, Physical Chemistry Chemical Physics 8 (2006) 5483–5500.
[57] S. Ivanova, V. Pitchon, V. Petit, V. Caps, ChemCatChem 2 (2010) 556–563.
[58] C. Rossignol, S. Arii, F. Morfin, L. Piccolo, V. Caps, J.-L. Rousset, Journal of Catalysis 230 (2005) 476–483.
[59] K. Qian, W. Zhang, H. Sun, J. Fang, B. He, Y.g. Ma, Z. Jiang, S. Wei, J. Yang, W. Huang, Journal of Catalysis 277 (2011) 95–103.
[60] S.-Y. Lai, Y. Qiu, S. Wang, Journal of Catalysis 237 (2006) 303–313.